

Synthesis and properties of Cr-Al-N films by a hybrid coating system with high power impulse magnetron sputtering (HIPIMS) and DC pulse sputtering

Min Su Kang^a, Tengfei Zhang^a, Dong-woo Shin^d, Qimin Wang^{b,c,*} and Kwang Ho Kim^{a,b,*}

^aSchool of Materials Science and Engineering, Pusan National University, Busan, 609-735, Korea

^bNational Core Research Center for Hybrid Materials Solution, Pusan National University, Busan, 609-735, Korea

^cSchool of Mechanical and Electronic Engineering, Guangzhou University of Technology, Guangzhou 510006, P.R. China

^dSchool of Nano & Advanced Materials Engineering, Gyeongsang National University, Jindaero 501, Jinju, Gyeongnam 660-701, Korea

CrN and CrAlN films were deposited on WC-Co, Si wafer and SUS 304 substrates by a hybrid coating system with high power impulse magnetron sputtering (HIPIMS) and pulsed DC sputtering. By varying the sputtering power of the Al target in the range of 0 A to 2.5 A, the Al content in the films increased from 0 to 17.7%. The effect of the Al content on the phase structure, mechanical properties and oxidation behavior of the films was investigated. The results indicated that the as-deposited CrAlN films possess the FCC structure of (Cr, Al)N phase. The hardness increased from 20.8 GPa for the CrN film to peak value of 25.4 GPa for the Cr_{0.28}Al_{0.14}N film and decreased with further increasing the Al content. The films with different Al content exhibited similar friction coefficients and wear behavior. The high-temperature oxidation resistance of the Cr_{0.28}Al_{0.14}N film was much better than that of the CrN film at 900-1000 °C.

Key words: Cr-Al-N films, HIPIMS, DC pulsed sputtering, High-temperature oxidation resistance.

Introduction

To increase the lifetime and performance of cutting and forming tools, there are increasing demands for protective coatings exhibiting high-temperature oxidation resistance as well as high hardness. As an important hard coating material, TiN has been widely used as the protective layer; however, it oxidizes at temperatures below 540 °C [1], which limits its applications in high-temperature environments such as high-speed cutting. It has been reported that the addition of Al improved the oxidation resistance of TiN films to around 800 °C [2, 3]. Together with high ductility, CrN films are also utilized as a hard, protective and wear resistant film for cutting tools, and show a significantly higher oxidation temperature than the TiN films [4, 5]. As the addition of Al improves the oxidation resistance of TiN films, a further improvement of oxidation resistance is expected by alloying Al in CrN films. However, relatively few research focusing on (Cr, Al)N films have been carried out [6, 7, 8], especially in terms of high-temperature oxidation resistance of the (Cr, Al)N films. It may be partly attributed to the difficulty in preparing dense (Cr, Al)N films. For instance, both AlN and CrN exhibit less electrical conductivity than TiN, which leads to microarcs caused by charge accumulation [6]. The arcing

phenomena severely degrades film quality, even destroys some electrical components of the controlling system [9].

HIPIMS stands for high power impulse magnetron sputtering. First publications go back to Vladimir Kouznetsov [10]. A comprehensive recent scientific survey has been published by Ulf Helmersson et al. [11]. Although pulse sputtering has already been known for some time, HIPIMS represents a remarkable innovation in the field of today's coating technology. In comparison to the conventional pulse-sputtering technologies, HIPIMS pulses gain average pulse energy of 2 to 6 MW per pulse. Typical pulse parameters exhibit peak voltages of 1.2-2 kV and peak currents between 0.5 and 4 kA, depending on the power rating of the DC-power supply. It is very important, that the pulse current density with reference to the total cathode area reaches at least 1 A/cm². The pulse duration and repeat frequency range between 15 to 200 μs and 50 to 200 Hz respectively. Employing these parameters during sputtering, a significant level of ionization of the sputtered atoms is observed, including multiple ionization [10], very similar as in case of cathodic arc evaporation, which leads to films with better quality.

In this study, CrAlN films are synthesized by a hybrid coating system with a HIPIMS using Cr source and a DC pulse sputtering using Al source. The influences of the DC pulsed power on the chemical composition, phase structure, wear behavior and mechanical properties of the films are investigated by varying the DC pulse power from 0 A to 2.5 A. Also,

*Corresponding author:

Tel : +82-51-510-2391

Fax: +82-51-510-3660

E-mail: kwhokim@pusan.ac.kr, qmwang@pusan.ac.kr

the high-temperature oxidation resistance of the films was evaluated.

Experimental

Film deposition

CrAlN films were deposited by a hybrid coating system combining HIPIMS+ (Hauzer Techno Coating BV) and DC pulse sputtering system as schematically shown in Fig. 1. The experiment was performed using an HIPIMS+ with Cr target and pulse DC with Al target. The relative contents of Cr and Al can be controlled by adjusting the pulse DC power of Al target. A rotating sample holder was positioned in the center of the chamber, about 100 mm from the targets. A bias power supply was connected to the sample holder. WC-Co (for scratch test), SUS 304 stainless steels (for wear test) and Si wafers (for XRD, EPMA, TEM, residual stress analysis and oxidation test) were used as substrates. WC-Co substrates were polished to have low surface roughness. And then all substrates were ultrasonically cleaned in acetone and ethyl ethanol sequentially for 30 min. They were then blown dry with N₂ and are put onto the holder. The chamber was evacuated to a base pressure below 5.0×10^{-5} torr using a rotary and turbo molecule pump. Before deposition, plasma etching was conducted by Ar glow discharge for 5 min with a DC bias of -700 V at 3.0×10^{-3} torr. Then ion bombardment was also conducted by the HIPIMS+ discharge of the Cr target for 5 min with a DC bias of -400 V at 3.2×10^{-3} torr. For increasing adhesion of films, Cr and CrN layer were deposited for 5 min, respectively. The working pressure was maintained at 3.0×10^{-3} torr and the ratio between the reactive gas N₂ pressure and inert gas Ar pressure was 2:1. The frequency of HIPIMS+ and duty cycle of the

DC pulse power was maintained at 30 Hz and 50%, respectively. While keeping other parameters constant, the DC pulsed power was changed from 0 A to 2.5 A to see its effects on film structures and properties. The deposition time was 240 min and deposition temperature is maintained about 300 °C. The sample holder rotated continuously at 1000 rpm during the deposition. The DC bias voltage was kept at -50 V. No apparent micro-arcs were observed during all the deposition processes.

Characterizations

The crystal structure of the films was determined by X-ray diffraction (XRD, D8-Discovery Bruker, Cu K α , 40 kV, 40 mA). Diffraction patterns were collected from 20 ° to 80 °. Surface and cross-section morphologies of the as-deposited and after oxidation test films were characterized by a scanning electron microscopy (SEM, S 4800, Hitachi) fitted with an EDX system accessory. The compositional analyses of films were carried out using an electron probe microanalyzer (EPMA 1600, Shimadzu). The selected coating was observed using a field emission transmission electron microscope (FE-TEM, JEOL, JEM-400FX) with an accelerating voltage of 400 kV. The hardness was evaluated by a microhardness tester with a Knoop indenter (Matsuzawa, MMT-7) under a load of 25 g. The friction coefficient was evaluated through sliding wear test using a conventional ball-on-disk wear apparatus. A steel ball (diameter 6.34 mm, 700 Hv_{0.2}) was used as a counterpart material. The sliding tests were conducted with a sliding speed of 0.157 m/s under a load of 3 N at ambient temperature (around 18 °C) and a relative humidity of 13~16%.

Results and discussion

Chemical composition, phase structure and microstructure of the CrAlN films

The CrAlN films with three different Al ratios from 7% to 17.7% and traditional CrN films were successfully deposited. The relative composition of the CrAlN films determined by EPMA was shown in Fig. 2. Fig. 3 shows the XRD patterns of the CrAlN films deposited on silicon wafer with various Al contents and the CrN film for comparison. The XRD peaks in the CrN film exhibited a pattern of the FCC crystal structure of CrN phase with the highest intensity of (111) plane. The peak intensity of (200) and (220) planes increased when Al content increased to 7-17.7 %. As compared to the CrN film, the CrAlN films exhibited apparently broadening diffraction peaks with reduced intensity. Also the diffraction peaks in the CrAlN films were shifted towards higher diffraction angle as the Al content increased. These results suggested that the lattice structure of CrAlN films formed a solid solution with Cr atoms substituted by Al atoms. Since the covalent radius of Al (0.121 nm) is smaller than that of Cr (0.139 nm), the shift of the diffraction peaks of the

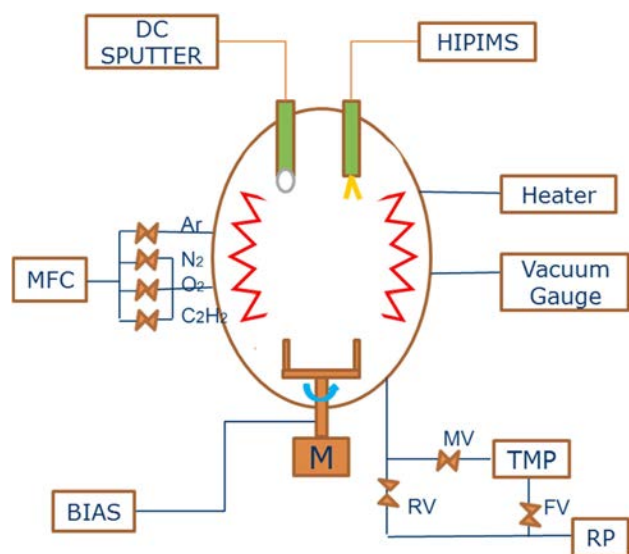


Fig. 1. The schematic diagram of the hybrid coating system in this study.

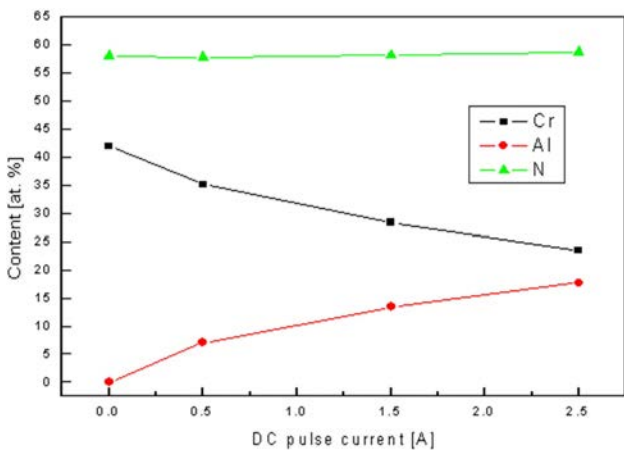


Fig. 2. EPMA profile as a function of DC pulse current.

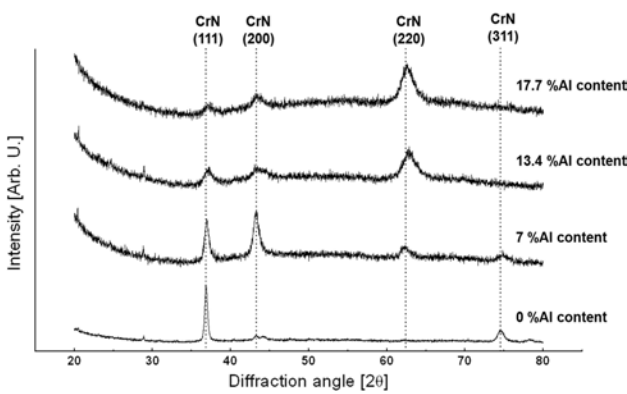


Fig. 3. XRD patterns of the Cr-Al-N films as a function of Al content.

films were observed for the films with higher Al contents. The peak broadening phenomenon and the decrease of the diffraction peaks intensity was caused by the decrease of the film crystallinity due to the incorporation of Al into CrN matrix.

In order to investigate the microstructure of the CrAlN films, high resolution TEM observations were

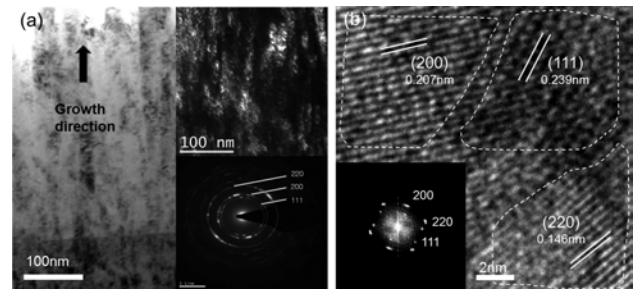


Fig. 4. (a) BF-TEM, DF-TEM (with SAED) and (b) HR-TEM (with SAED) images of Cr_{0.28}Al_{0.14}N coating.

performed on the CrAl (13.4%)N film. Fig. 4 shows the cross-sectional TEM images and corresponding electron diffraction patterns of the CrAl (13.4%)N film. From the bright field (BF-) and dark field (DF-) TEM image (Fig. 4(a)), the film layer was found to possess the columnar microstructure containing irregular nanograins. Fig. 4(a) also presents the selected area electron diffraction (SAED) pattern of the CrAl (13.4%)N film. The SAED pattern was constituted of polycrystalline rings superimposed with spots, indicating the existence of preferred orientation growth of crystals in the film [17]. The strong (111), (200) and (220) ring were observed, which was consistent with the results in Fig. 3. Combining the results of XRD and SAED pattern, it can be inferred that Al might form as a solid solution of (Cr, Al)N phase in the CrAlN films. Fig. 4(b) shows the HR-TEM image in the middle regions of Fig. 4(a). Some nanograins with (111), (200) and (220) orientations were observed. The results are consistent with the BF-TEM image and SAED pattern in Fig. 4(a).

Mechanical properties of CrAlN films

The hardness values of the as-deposited films were shown in Fig. 5(a). All the CrAlN films showed significantly higher hardness as compared to the CrN film. With increasing the Al content to 13.4%, the

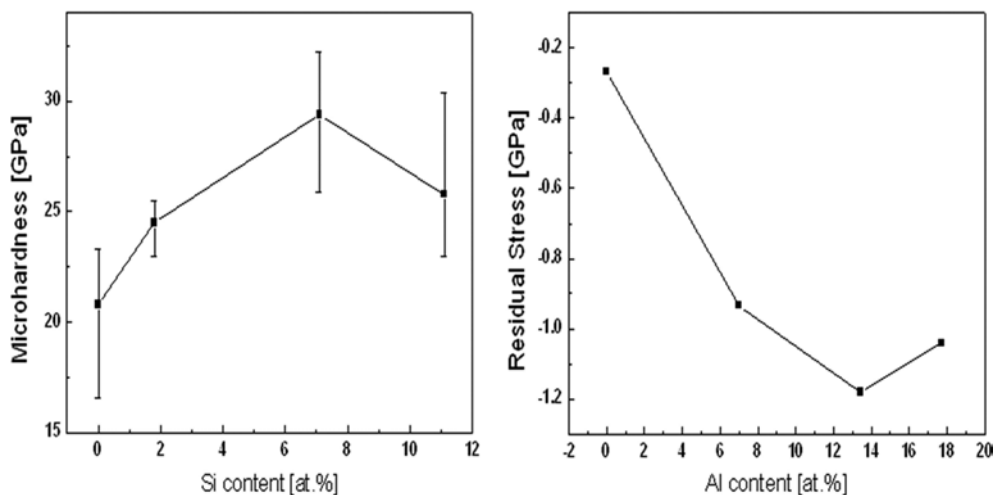


Fig. 5. (a) Microhardness and (b) residual stress of the Cr-Al-N films as a function of Al content.

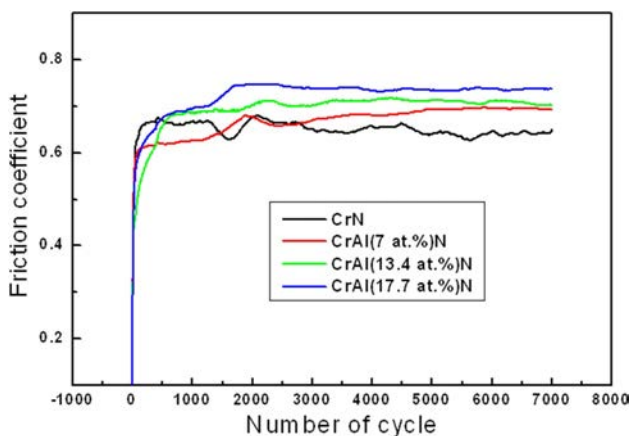


Fig. 6. Average friction coefficient of the Cr-Al-N films as a function of Al content.

hardness of the films increased from 20.8 GPa to 25.4 GPa. The greatly enhanced mechanical properties of CrAlN films can be explained by solid solution hardening and complex chemical bonding strengthening. An explanation of the high hardness of the CrAlN films was the local bond strengthening and dislocation motion hindered by lattice distortion. By taking into account the bonding characteristics and assuming that the bulk modulus increases when the interatomic distance in AB compounds reduces [12, 13], it can be suggested that the increase of hardness in CrAlN films also originates from the decrease of the nearest neighbor distance. The fact that the lattice parameter

and elastic modulus correlates with the hardness values also indicates that the nature of bonding in the CrN host lattice is modified by the introduction of Al atoms with a smaller atomic radius and different electronic structure. And the hardness of the CrAlN films is partially determined by solid solution hardening and complex chemical bonding strengthening. The dislocation mobility depends on the chemical bonding. Fig. 5b shows the residual stress data plotted at various Al contents of CrAlN films. The residual stress changed from -0.27 GPa to -1.18 GPa with increasing the Al content from 0 to 13.7 at.% for the CrAlN films. The residual stresses rebounded with further increase of the Al contents. This phenomenon can be explained by the microstructural defects which formed due to substitutional replacement of Al ($r=1.43 \text{ \AA}$) atoms for Cr ($r=1.85 \text{ \AA}$) sites in the films and played as a barrier to dislocation propagation.

Fig. 6 shows the friction coefficient of CrAlN coatings as a function of the Al content under a normal load of 3N at ambient temperature (about 18 °C) and a relative humidity of 13~16%. The films with various Al contents exhibited very similar average friction coefficients, only slightly increased from 0.6 to 0.75 with increasing Al content. Fig. 7 shows SEM morphologies of the wear tracks after sliding test. As the Al content increased, the wear track morphology became rougher.

Fig. 8 and Fig. 9 show the typical friction-load curve and optical micrographs of scratch measured by scratch tester. Generally, the scratch test includes three stages:

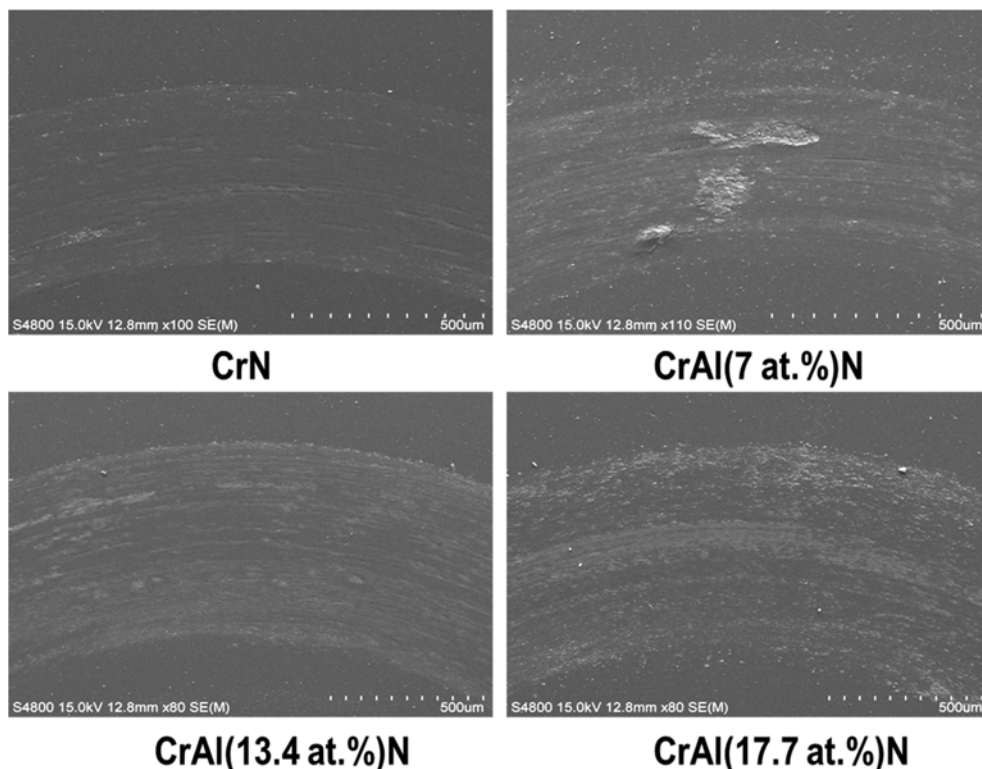


Fig. 7. SEM morphologies of the wear tracks after sliding tests.

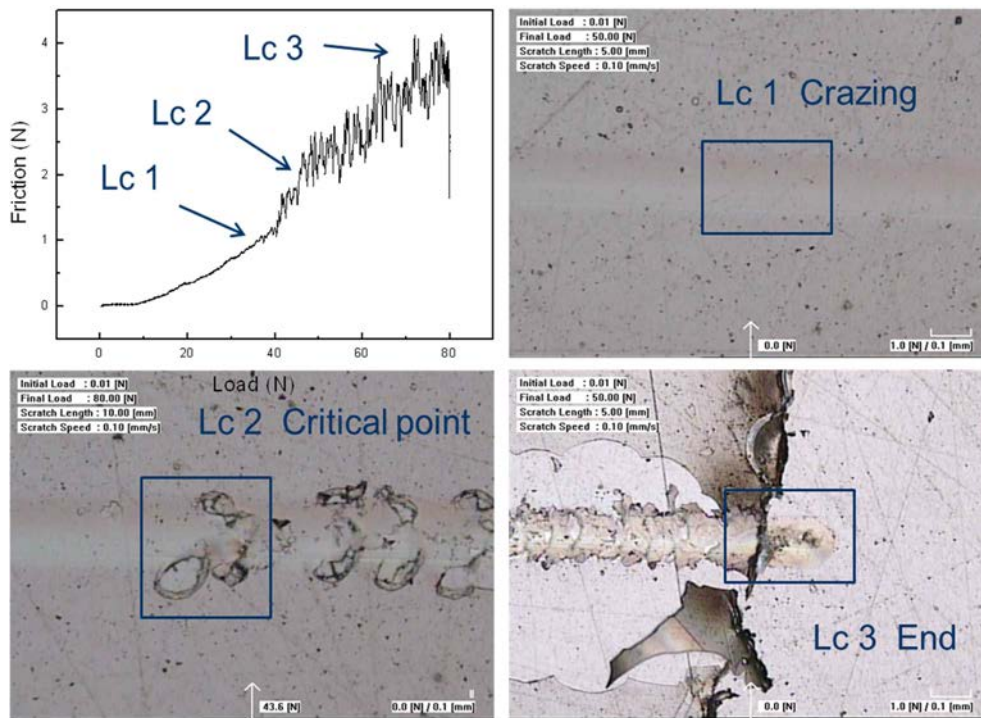


Fig. 8. The scratch test curves and optical scratch images of the CrN film.

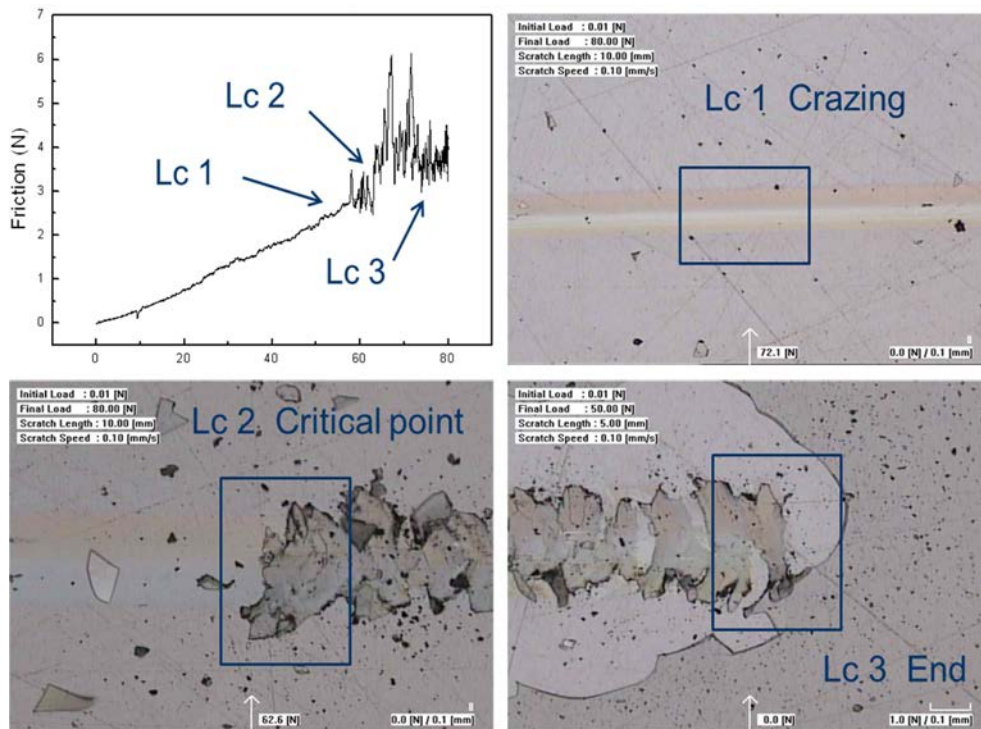


Fig. 9. The scratch test curves and optical scratch images of the Cr-Al-N film.

the fine cracks stage (critical load denoted as Lc 1) with an oscillation of the friction, the peeling off stage (critical load denoted as Lc 2) with a rapid increase of the friction, and the complete peeling off stage (critical load denoted as Lc 3). The second stage was regarded as a sign of coatings adhesion failure, which was

defined as adhesion strength [16]. As shown in Fig. 8, Lc 1 was found to be 40 N. Fig. 8 (Lc 1) shows the optical images of the scratch scar at the Lc 1 point of CrN films, from which the fine cracks could be seen. With further increasing load, the inflection point of the friction-load curve and the increase of the friction

appeared at the Lc2 of 50 N. Fig. 8(Lc 2) shows the critical point of spallation and peeling. The high oscillation and high slope of friction-load curve appeared at the position of Lc 3. Fig. 8 (Lc 3) shows the scratch scar picture at the Lc 3 point, where the fragments are observed on both sides of the scratch. As a result, the adhesion strength of the CrN film was 50 N at the position of Lc 2. On the other hand, Fig. 9 shows result of scratch test of CrAl(13.4%)N films. As shown in Fig. 9, the adhesion strength of the CrAl(13.4%)N film was 60 N at the position of Lc 2, which is higher

than that of the CrN film.

High-temperature oxidation resistance of CrAlN films

Fig. 10 shows the cross-sectional SEM images of the CrN and CrAlN films after oxidation test. After annealing at 900 °C and 1000 °C in air for 1 h and 2 h, there was an apparent change in the microstructure of the CrN coating. The fractured cross sectional image of the CrN film at 900 °C for 1h (Fig. 10(a)) exhibited an oxide layer more than 5 μm and loose columnar grains

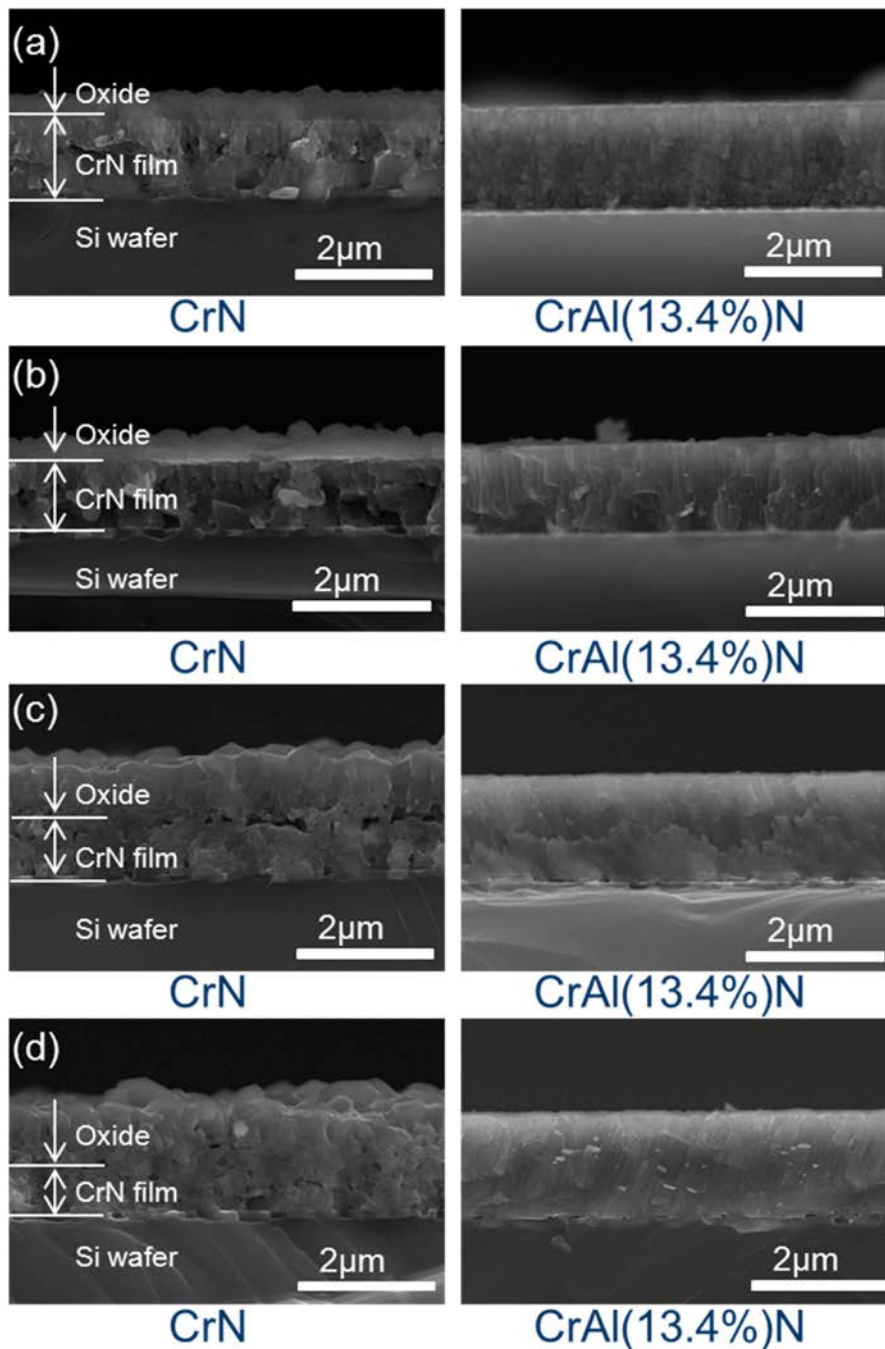


Fig. 10. Cross-sectional SEM images of the CrN and Cr-Al-N films after annealing in air at (a) 900 °C for 1 h, (b) 900 °C for 2 h, (c) 1000 °C for 1 h, (d) 1000 °C for 2 h.

beneath the oxide layer. On the other hand, CrAl(13.4%)N film after 900 °C in air for 1h still exhibited dense columnar structure without visible change. No apparent oxide layer was detected in CrAl(13.4%)N film. As shown in Fig. 10(b), oxidation CrN and CrAl(13.4%)N films was more progressed after 900 °C for 2 h oxidation than that after oxidation for 1h. The oxide layer on the CrN film surface thickened while still no apparent oxide layer formed on the CrAl(13.4%)N film. For the more severe environment at 1000 °C in air (Fig. 10(c), Fig. 10(d)), the cross sectional view of the CrN film revealed a porous morphology because of oxidation. Nevertheless, the CrAl(13.4%)N film still maintained dense columnar structure and no apparent oxide layer can be detected on the film surface, which revealed much better oxidation resistance than that the CrN film.

Conclusion

Ternary CrAlN films were deposited on WC-Co, SUS 304 stainless steel substrates and Si wafer by a hybrid coating system using HIPIMS+ and DC pulse sputtering. The chemical compositions, microstructures, mechanical properties and oxidation behavior of the CrN and CrAlN films were investigated. The results revealed that the CrAlN films consisted nano-sized (Cr,Al)N crystals. The CrAlN films exhibited a maximum hardness of ~ 25.4 GPa for the Cr_{0.28}Al_{0.14}N film due to the solid-solution hardening. The Cr_{0.28}Al_{0.14}N film also exhibited the lowest negative value of residual stress. The friction coefficients of the CrAlN films were very similar to that of the CrN film. The Cr_{0.28}Al_{0.14}N film had adhesion strength of 60 N, a bit higher than that of the CrN film (40 N). During the oxidation tests at 900 and 1000 °C, the Cr_{0.28}Al_{0.14}N film exhibited much better oxidation resistance than the CrN film.

Acknowledgement

This work was supported by NCRC (National Core Research Center) program (2011-0006-256) through the National Research Foundation of Korea funded by the Ministry of Education, Science and Technology.

References

1. E. Erturk, H. Haessler, *Thin Solid Films* 153 (1987) 433.
2. W.D. Munz, *J. Vac. Sci. Technol.*, A 4 (1986) 2717.
3. T. Ikeda, H. Satoh, *Thin Solid films* 195 (1991) 99.
4. M.A. Baker, P.J. Kench, M.C. Joseph, C. Tsotsos, A. Leyland, A. Matthews, *Surf. Coat. Technol.* 162 (2003) 222.
5. H. Ichimura, A. Kawana, *J. Mater. Res.* 9 (1994) 151.
6. O. Knotek, F. Loeffler, H. Scholl, *Surf. Coat. Technol.* 45 (1991) 53.
7. E. Lugscheider, K. Bobzin, Th. Hornig, M. Mases, *Thin Solid Films* 420-421 (2002) 318.
8. H.C. Barshilia, B. Deepthi, N. Selvakumar, A. Jain, K.S. Rajam, *Appl. Surf. Sci.* 253 (2007) 5076.
9. A. Anders, *Thin Solid Films* 502 (2006) 22.
10. V. Kouznetsov, K. Macak, J.M. Schneider, U. Helmersson, I. Petrov, *Surf. Coat. Technol.* 122 (2-2), (1999) 290.
11. U. Helmersson, M. Lattemann, J. Bohlmark, A.P. Ehasarian, J.T. Gudmundsson, *Thin Solid Films* 513, Issues 1-2, (2006), 1-24.
12. M.L. Cohen, *Phys. Rev. B* 32 (1985) 7988.
13. M. Zhou, Y. Makino, M. Nose, K. Nogi, *Thin Solid Films* 339 (1999) 203.
14. M. Zhang, G. Lin, G. Lu, C. Dong, K.H. Kim, *Appl. Surf. Sci.* 254 (2008) 7149-7154.
15. L. Wang, G. Zhang, R.J.K. Wood, S.C. Wang, Q. Xue, *Surf. Coat. Technol.* 204 (2010) 3517-3524.
16. T. Li, M. Li, Y. Zhou, *Surf. Coat. Technol.* 201 (2007) 7692.
17. S.K. Kim, V.V. Le, P.V. Vinh, J.W. Lee, *Surf. Coat. Technol.* 202 (2008) 540.